

# Difference-based Deep Convolutional Neural Network for Simulation-to-reality UAV Fault Diagnosis

Wei Zhang, Junjie Tong, Fang Liao and Yunfeng Zhang

**Abstract**—Identifying the fault in propellers is important to keep quadrotors operating safely and efficiently. The simulation-to-reality (sim-to-real) UAV fault diagnosis methods provide a cost-effective and safe approach to detect the propeller faults. However, due to the gap between simulation and reality, classifiers trained with simulated data usually underperform in real flights. In this work, a new deep neural network (DNN) model is presented to address the above issue. It uses the difference features extracted by deep convolutional neural networks (DD-CNN) to reduce the sim-to-real gap. Moreover, a new domain adaptation method is presented to further bring the distribution of the real-flight data closer to that of the simulation data. The experimental results show that the proposed approach can achieve an accuracy of 97.9% in detecting propeller faults in real flight. Feature visualization was performed to help better understand our DDCNN model.

**Index Terms**—Intelligent fault diagnosis; Difference features; Simulation-to-reality; Domain adaptation;

## I. INTRODUCTION

QUADROTOR unmanned aerial vehicles (UAVs), become increasingly popular in various fields, such as search-and-rescue and homeland security [1]. However, their propellers may be vulnerable to damage during operation (see Fig. 1) due to unforeseen events, such as collisions with buildings or trees. Such damage can impede the UAV's capability to accomplish its mission and may even lead to significant damage to the UAV itself and to people in the surrounding area. Hence, it is essential to keep monitoring the conditions of quadrotor propellers. Identifying propeller problems at an early stage allows for a timely recall of the UAVs, and hence reducing further damages.



Fig. 1. Example of broken propeller.

Based on the use of system models or not, UAV fault diagnosis methods can be divided into model-based and model-free methods. The model-based approach [2], [3] requires

(Corresponding author: Junjie Tong.)

Wei Zhang, Junjie Tong and Yunfeng Zhang are with the Department of Mechanical Engineering, National University of Singapore. e-mail: weizhang@u.nus.edu, tongjj@nus.edu.sg, mpezyf@nus.edu.sg

Fang Liao are with Temasek Laboratories, National University of Singapore, Singapore. e-mail: tsllf@nus.edu.sg

first building a model of the system and then comparing the model output with the actual output to identify propeller failures. Therefore, an accurate system model of a real UAV is the key to successful fault diagnosis. However, due to noise and installation errors, building an accurate system is not trivial and requires a much expert knowledge and performing extensive experiments.

Compared with model-based approaches, the model-free methods do not rely on an system model. Among model-free approaches, data-driven approaches [4], [5] have become increasingly popular in recent years. These approaches utilize flying data and fault labels to train a fault classifier. The fault classifier is built on deep neural networks (DNNs) [6], which can extract features from the sensor's input and perform classification simultaneously. Such end-to-end mechanism bypasses the model building process and therefore does not require much knowledge of UAV system.

In contrast to other data-driven fault diagnosis fields, such as bearing fault diagnosis [7], the collection of UAV fault is difficult because flying with broken propeller can result in a drone crash. To reduce the risk of real-world data collection, it is a safer approach to collect training data in a simulation and then deploy the well-trained classifier to a real UAV. Such approach is also referred to as simulation-to-reality (sim-to-real), which is a common approach to learn data-driven controllers for robots [8]. However, due to noise and mounting errors, a simulated drone cannot have the same behavior as a real drone under the same commands, which poses a challenge for a fault classifier trained with simulated data.

In this research, we focus on developing a data-driven classifier that can bridge the sim-to-real gap and achieve high fault-diagnosis accuracy in real flight. To reach this goal, we propose the difference-based convolutional neural network (DDCNN) that learns difference features from the tested sample and all-healthy category. Although the difference features are learned from simulated data, they can generalize well in real flight. Moreover, a simple but effective domain adaptation (DA) method is presented to align the distribution of the all-healthy samples from simulation and real flight. It can further reduce the sim-to-real gap and improve the classification performance. To sum up, the contributions of this work are as follows,

- The DDCNN model is proposed to reduce the sim-to-real gap and improve the performance of the classifier in real flight.

- A new DA method is presented to further reduce the sim-to-real gap for the DDCNN model.
- Using DDCNN and DA, a propeller fault classifier trained with simulated data can achieve high accuracy in diagnosing UAV fault using real flight data.

The rest of this paper is structured as follows. A brief summary of related works is given in Section II, then the problem description is presented in Section III. The proposed DDCNN model and DA methods are introduced in Section IV, followed by the model training and performance evaluation of our method in Section V. Last, we draw conclusions in Section VI.

## II. RELATED WORKS

### A. Data-driven UAV fault diagnosis

Data-driven UAV fault diagnosis approaches train DNNs as classifiers to learn fault diagnosis skill from the manually-labelled flying data. The flying data usually contains the state information, such as roll, pitch yaw, angular velocities and accelerations, and the rotational speeds of propellers. A new DDN model named deep residual shrinkage network was presented for UAV fault diagnosis [9]. Trained with real flight data, the classifier can perform accurate fault diagnosis on the test data collected from the same flights. Similarly, Park et al. [5] proposed the stacked pruning sparse denoising auto-encoder for UAV fault diagnosis. Due to the use of denoising auto-encoder, the classifier performed well in the noisy scenario.

Instead of using the state information of the UAV as input, the audio signal received by an external microphone array can also be used for fault diagnosis task. Katta et al. [10] adopted convolutional neural networks (CNNs) [11] and transformer [12] encoders to classify the Mel-frequency cepstral coefficient (MFCC) features of audio signals into the fault type. However, all these approaches cannot avoid the use of broken drones for real-world data collection, which is dangerous due to the unexpected behavior of broken drones.

### B. Sim-to-real transfer of DNNs

Although sim-to-real transfer is new in UAV fault diagnosis domain, it has gained much attention from other fields, especially in robot control [13]. Zhang et al. [14] trained a mobile robot using LiDAR as a distance sensor in a simulated scenario, and the trained DNN controller can control the robot in the real world with different LiDAR configurations. For quadrotors, Rubi et al. [15] trained a quadrotor to learn path-following and obstacle-avoidance tasks in simulation, and the trained model can be used by a real quadrotor. However, for the above approaches, the gap between simulation and reality is small due to the high-fidelity LiDAR sensors in the simulation. Therefore, the DNN controller trained in the simulation can be deployed directly to the real robot.

For vision-based sim-to-real robot control, the robot's observations in simulation may differ from those in the real world [16]. To reduce the gap between simulation and reality, the domain randomization method for sim-to-real drone race task

was presented [17]. However, for our UAV fault diagnosis task, the sim-to-real gap is mainly caused by differences in the UAV body, i.e., mounting errors and noise, rather than by observations received by the on-board sensors.

## III. PRELIMINARIES

First of all, abbreviations which are frequently used in this work are summarized in Table I.

TABLE I  
ABBREVIATIONS AND DESCRIPTIONS

Abbreviation	Description
DA	Domain adaptation
DCNN	Deep convolutional neural network
DDCNN	Difference-based Deep convolutional neural network
t-SNE	t-distributed stochastic neighbor embedding

### A. Problem description

The quadrotor propeller fault diagnosis problem can be model as a classification problem. In this problem, there are five categories, including one all-healthy category and four fault categories, which are listed in Table II. The input to the classifier is consisted of the flying data of the quadrotor. In this paper, at step time  $t$ , the input  $x_t$  comprise the angular accelerations and the square of the rotational speed of the propellers as follows,

$$x_t = \begin{bmatrix} \dot{p}_{t-T} & \dot{p}_{t-T+1} & \cdots & \dot{p}_t \\ \dot{q}_{t-T} & \dot{q}_{t-T+1} & \cdots & \dot{q}_t \\ \dot{r}_{t-T} & \dot{r}_{t-T+1} & \cdots & \dot{r}_t \\ \omega_{1,t-T}^2 & \omega_{1,t-T+1}^2 & \cdots & \omega_{1,t}^2 \\ \omega_{2,t-T}^2 & \omega_{2,t-T+1}^2 & \cdots & \omega_{2,t}^2 \\ \omega_{3,t-T}^2 & \omega_{3,t-T+1}^2 & \cdots & \omega_{3,t}^2 \\ \omega_{4,t-T}^2 & \omega_{4,t-T+1}^2 & \cdots & \omega_{4,t}^2 \end{bmatrix}. \quad (1)$$

where  $(\dot{p}, \dot{q}, \dot{r})$  denotes quadrotor angular accelerations;  $\omega_{i=1,2,3,4}$  denote the rotational speeds of four propellers.  $T$  is time-window length. It determines how much historical information is taken into account in the input. The purpose of the classifier is to label the input sample based on their output as one of the five categories.

TABLE II  
LABELS OF FIVE FAULT CATEGORIES.

label*	Propeller 1	Propeller 2	Propeller 3	Propeller 4
1	healthy	healthy	healthy	healthy
2	faulty	healthy	healthy	healthy
3	healthy	faulty	healthy	healthy
4	healthy	healthy	faulty	healthy
5	healthy	healthy	healthy	faulty

In this work, the classifier can only be trained with samples generated in simulation and all-healthy samples from real flight, because recording samples with broken propeller from real flight is dangerous. Once trained, the classifier will be employed to detect fault for real flight. Hence, the classification problem in this task is a sim-to-real classification problem. Sim-to-real classification problem can be viewed as

cross-domain classification problem. The simulation domain is considered as source domain, while the real-world domain is regarded as target domain. This cross-domain classification problem is challenging because of the domain gap induced by noise and installation error. The objective of this paper is to train a classifier with simulated data to achieve high accuracy on real flight data.

#### IV. APPROACH

In this section, a new method for monitoring the health condition of quadrotor propellers is presented. The overall framework of the proposed approach is given in Fig. 2. As shown, DDCNN is proposed as the fault classifier. The training data comprises simulated flight data and all-healthy samples collected from one individual flight. To enhance the generalization capability of the DDCNN model in actual flight, a new domain adaptation method is introduced. Once trained, the DDCNN model can be employed to monitor the status of the UAV in real-world situations.

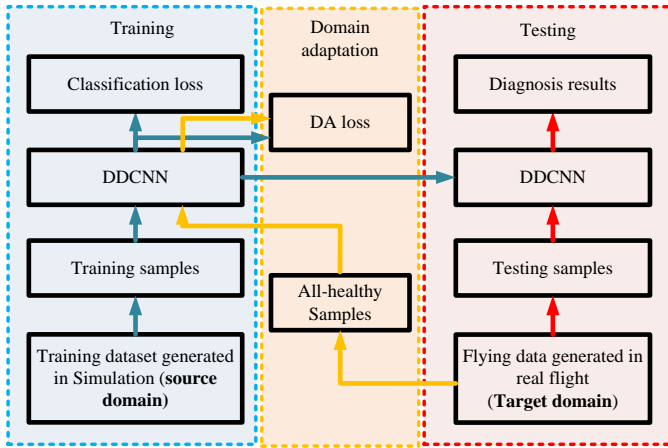


Fig. 2. Framework of the proposed approach.

##### A. DDCNN model

The architecture of the DDCNN model is depicted in Fig. 3. As shown, similar to Siamese neural network [18], it contains two identical deep convolutional neural networks (DCNNs), namely DCNN\_1 and DCNN\_2, parameterized by  $\phi_1$ ,  $\phi_2$ , respectively. In other words, DCNN\_1 and DCNN\_2 share the same network structure and weights, i.e.,  $\phi_1 = \phi_2$ . As shown in Fig. 3a, the DCNN models contains three convolutional layers. After each convolutional layer, a max-pooling operation is performed. The features learned by the convolutional layers are flattened and fed into a fully-connected layer. The 1D vector outputted by the fully-connected layer is treated as the features of the input sample. Due to domain change, the features of the same-category samples from different domain, i.e., simulation and real flight, are different. However, the differences between the faulty features and the all-healthy features can be similar in different domain. Hence, our DDCNN model is under the following assumption.

*Assumption 1:* The differences between faulty features and all-healthy features are similar in different domain.

With Assumption 1, the features used for fault classification are the differences between the features of the diagnosed sample and the features of the all-healthy category. The calculations of the difference features  $\phi_d$  vary in training and testing phases. During training, as shown in Fig. 3b, the input to DCNN\_1, i.e.,  $x_i$ , is the training samples sampled from any fault categories, while the input to DCNN\_2, i.e.,  $x_j$ , is the training samples sampled from the all-healthy category. After forward propagation in each DCNN, the difference features  $\phi_{d,train}$  used in training are calculated as follows,

$$\phi_{d,train} = \tanh(\phi_1(x_i) - \phi_2(x_j)) \quad (2)$$

where  $\phi_1(x_i)$  denotes the features outputted by the DCNN\_1 on sample  $x_i$ ;  $\phi_2(x_j)$  represents the features outputted by the DCNN\_2 on sample  $x_j$ .  $\tanh(\cdot)$  is the tanh activation function, which controls the range of each difference feature be  $(-1, 1)$ .

With the difference features  $\phi_d$ , as shown in Fig. 3b and 3c, a classifier with two hidden fully-connected layers are used to compute the probability of each fault type. The output layer utilizes the Softmax function to transform the logits of the five neurons into discrete probability distributions representing the five possible quadrotor health conditions. The formula for the Softmax function is as follows:

$$q(z_j) = \text{softmax}(z_j) = \frac{e^{z_j}}{\sum_{i=1}^5 e^{z_i}} \quad (3)$$

where  $z_j$  denotes the logits of the  $j$ -th output neuron.

The classification loss for training the DDCNN model is the cross-entropy loss between the estimated softmax output probability distribution and the target class probability distribution. Let  $p(x)$  denote the target distribution and  $q(x)$  denote the estimated distribution outputted by DCNN, the cross-entropy loss  $\mathcal{L}_c$  between  $p(x)$  and  $q(x)$  is:

$$\mathcal{L}_c = H(p(x), q(x)) = -\sum_x p(x) \log q(x). \quad (4)$$

##### B. Domain adaptation based regularization

When a fault classifier is utilized for fault diagnosis, its performance may be compromised due to the different distributions of the target and source domain data. To address this issue, domain adaptation (DA) methods are frequently employed to align the distribution of the target domain data with that of the source domain data. However, typical DA approaches require access to the full range of unlabeled data from the target domain, which is not feasible in our case due to the risks associated with flying a quadrotor with a broken propeller. Therefore, our DA method aims to utilize only the all-healthy samples from the target domain to extract transferable features, which allows for a safer approach. Similar to [19], only the all-healthy samples from the target domain are utilized for DA. Our DA method is under the following assumption,

*Assumption 2:* The cross-domain variation way for samples of different faults is similar.

Under the assumption that the distributions of healthy source and target domain data are brought closer together, it is possible to decrease the distance between the source and

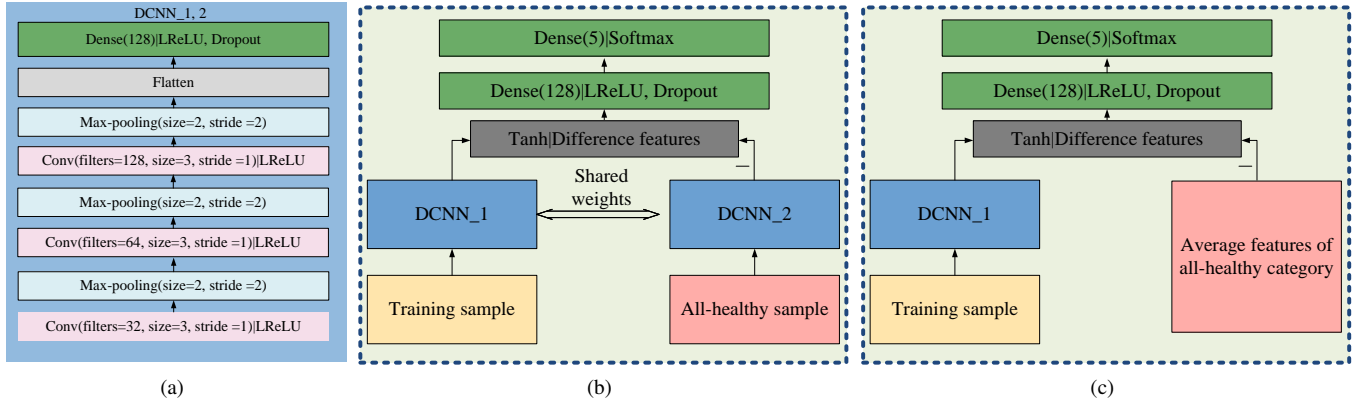


Fig. 3. Network structure of DDCNN. (a) the network structure of DCNN\_1 and DCNN\_2. (b) the network structure of DDCNN used for training. (c) the network structure of DDCNN used for testing.

target domain distributions of other categories. In this paper, the difference features in DDCNN serves as the features to perform domain adaptation. Due to the use of the difference features, the target distribution of the features in both domains are zero-centered. Hence, different from [19], we do not need to calculate the domain distance, such as MMD (Maximum Mean Discrepancy) distance, and minimize the domain distance. In this paper, we only need to make each element of the difference features be zero, and the DA loss used in this paper is shown as follows,

$$\mathcal{L}_{DA} = \left\| \frac{1}{n_{AH}} \sum_{x_j \in \mathcal{X}_{AH}} \phi_d(x) \right\|_2^2. \quad (5)$$

Minimize the DA loss can make the difference features of all-healthy samples in target domain closer to zero and their distribution closer to that of all-healthy samples in source domain. By integrating the classification loss and DA loss together, the model loss function is as follows,

$$\mathcal{L} = \mathcal{L}_c + \lambda \mathcal{L}_{DA} \quad (6)$$

where the factor  $\lambda$  is a constant which weighs the contribution of the DA loss.

### C. Difference features in testing

During testing, as shown in Fig. 3b, the input  $x_i$  to DCNN\_1 is the sample to be tested (this sample can be from any fault categories), while DCNN\_2 and its input are replaced by the pre-computed feature representation  $\bar{\phi}_2$ .  $\bar{\phi}_2$  represent the features of the all-healthy category extracted by DCNN\_2. Hence, the difference features calculated during testing are as follows,

$$\phi_{d,test} = \tanh(\phi_1(x_i) - \bar{\phi}_2) \quad (7)$$

In this paper,  $\bar{\phi}_2$  is estimated using the average features of the all-healthy samples as follows,

$$\bar{\phi}_2 = \frac{1}{n_{AH}} \sum_{x_j \in \mathcal{X}_{AH}} \phi_2(x_j) \quad (8)$$

where  $\mathcal{X}_{AH}$  denotes the group of the all-healthy samples, which can be collected from an individual flight.  $n_{AH}$  is the

---

### Algorithm 1: Training and testing procedure of DDCNN with Domain Adaptation

---

- 1 **Model Training;**
  - 2 Initialize parameters of DDCNN  $\theta$ ;
  - 3 Input: training Dataset A, all-healthy real-flight Dataset B, and testing Dataset C;
  - 4 Copy the all-healthy category in Dataset A and Dataset B into Dataset D and E;
  - 5 **for** epoch= 1, 2, ..., **do**
  - 6     **for** training step= 1, 2, ..., **do**
  - 7         Randomly sample  $m$  samples from Dataset A, B, D and E into a mini-batch  $\mathcal{M}_A$ ,  $\mathcal{M}_B$ ,  $\mathcal{M}_D$  and  $\mathcal{M}_E$ ;
  - 8         Calculating the cross entropy loss using  $\mathcal{M}_A$  and  $\mathcal{M}_D$  with eq. (4);
  - 9         Calculating the DA loss using  $\mathcal{M}_B$  and  $\mathcal{M}_E$  with eq. (5);
  - 10         Updating the  $\theta$  by minimizing total loss  $\mathcal{L}$  using gradient decent;
  - 11     **end**
  - 12 **end**
  - 13 **Model Testing;**
  - 14 Replace the DCNN\_2 with the average features of all-healthy category with eq. (8);
  - 15 Classify the testing samples in Dataset C using eq. (7) and eq. (3).
- 

number of samples in  $\mathcal{X}_{AH}$ . With eq. (7) and eq. (8), during testing, only the forward computation of  $\phi_1(x_i)$  is performed for calculating the difference features. With the training and testing details, the whole procedure of our algorithm can be found in Algorithm 1.

## V. IMPLEMENTATION AND TEST

In this section, we trained the DDCNN model and assess its sim-to-real performance using real flight data. The training data for the DDCNN model was generated using a simulation model presented in [20]. Once trained, the DDCNN model was applied to classify faults on real flight data.



### A. Dataset Description

As shown in Table III, three datasets, i.e., Dataset A, B and C, are generated or collected in this paper. Dataset A was generated in simulation using the simulator introduced in [20]. It covers five categories, and each category has 3000 samples. To collect samples for each fault category, the simulated UAV was required to fly to the designated waypoints using the onboard controller. The waypoints were the same for the five categories.

Besides, Dataset B was utilized for training as well. As shown in Fig. 4b, it was collected from a real flight under the all-healthy conditions. During data collection, a human pilot randomly flew the quadrotor in an indoor scenario for around five minutes. Accordingly, 3000 samples of the all-healthy category were collected. Dataset B is used for different purposes in training and testing. During training, it was used for performing domain adaptation. During testing, it was used to pre-compute the features for the real-world all-healthy category.

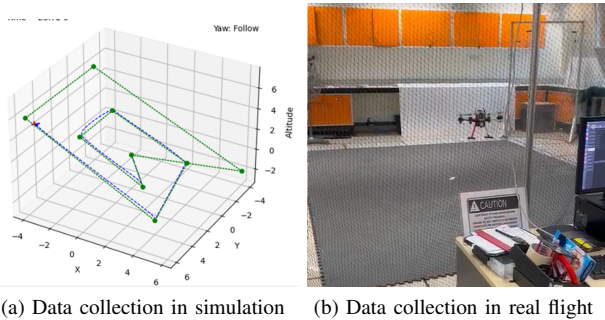


Fig. 4. Data collection in simulation and real flight.

Dataset C is the dataset used for testing. It was collected from real flight and contains five categories and has 800 samples in each category. The same as Dataset B, the UAV was controlled by a human pilot. The flying trajectories were different for each category, and each flight took about two minutes. Before collecting the data with each faulty category, one healthy propeller was replaced by a broken propeller in the labelled position as shown in Fig. 5. It should be noted that the damaged levels of the broken propellers in the four positions are different.

### B. Training details

As the proposed model mainly utilizes DDCNN model and DA-based regularization, we refer to our model as DDCNN+DA model. Besides, to evaluate the effect of the proposed DA method, the DDCNN model without DA is also trained and tested. Moreover, to evaluate the effect of the difference features in DDCNN, we remove the difference operation in the DDCNN model, i.e., the DCNN\_2 branch is removed in Fig 3b, and refer to this model as DCNN model. The DCNN model with DA was not implemented because the presented DA method relies on the difference features of DDCNN model, which is not suitable for DCNN model.

The hyperparameters of training are listed in Table IV. The GPU used for training is RTX 2080Ti, which took about

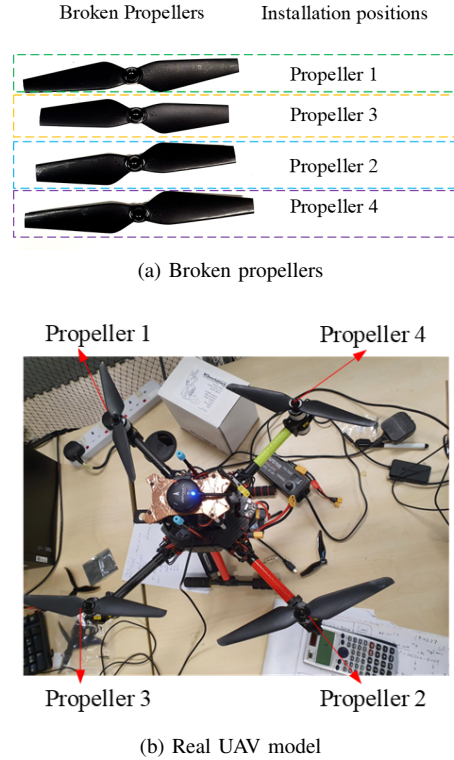


Fig. 5. The real UAV model and broken propellers used in real-world data collection.

two minutes for each training process. The training process was repeated five times using different random seeds to assess the robustness and repeatability of each model.

### C. Results and comparison study

Once trained, the DDCNN+DA model can be employed for fault classification tasks. The classification accuracy of the model DCNN, DDCNN and DDCNN+DA on the training Dataset A and testing Dataset C are summarized in Fig. 6. As shown, The value of each column indicates the mean accuracy of five runs, while the corresponding standard deviation of five accuracies is also plotted on the top of each column.

It can be seen that the DCNN model can only achieve an average accuracy of 56%, which indicates there exists a large gap between the simulated data and the real-flight data. With the help of the presented DDCNN model, the average accuracy increases to 84.8%, which is a huge performance improvement. It shows the difference features learned with simulation data remain useful for real flight data. Moreover, with the help of DA, the DDCNN model can achieve an average accuracy of 97.9%. This promising result demonstrates that the proposed DA method can further reduce the sim-to-real gap.

### D. Visualization of the difference features

To better understand the DDCNN+DA model, the difference features learned by DDCNN+DA on training Dataset A and testing Dataset C are plotted in Fig. 7. As shown, for each fault label, the solid line and the translucent area represents the average value and the standard deviation of the difference

TABLE III  
DESCRIPTION OF QUADROTOR DATASETS GENERATED FOR TRAINING AND TESTING.

Dataset Name	Data source	Purpose	Category label (fault location)				
			1 (None)	2 (Propeller 1)	3 (Propeller 2)	4 (Propeller 3)	5 (propeller 4)
			Number of samples				
A	Simulation	Training	3000	3000	3000	3000	3000
B	Real flight	Training	3000	-	-	-	-
C	Real flight	Testing	800	800	800	800	800

TABLE IV  
HYPERPARAMETER SETTINGS.

Hyperparameters	Value
Mini-batch size	128
Learning rate	$5 \times 10^{-4}$
Maximum training epochs	10
Optimizer	Adam
Dropout rate	20%
Factor of DA loss: $\lambda$	0.1

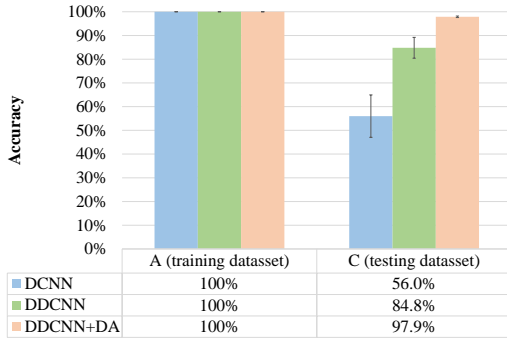


Fig. 6. Accuracy of the DCNN, DDCNN and DDCNN+DA on the training Dataset A (simulation) and testing Dataset C (real flight).

features calculated on 3000 training samples (in blue) and 800 testing samples (in red), respectively. It should be noted that the difference features used in testing for the training samples are the average features of the all-healthy training samples.

As shown, the difference features of the test samples overlap well with the corresponding features of the training samples, which explains why the DDCNN+DA model achieves high accuracy on the testing dataset. Besides, the training and testing features of the all-healthy category (Label 1) are all around zero, which is consistent with eq. (7) and eq. (8). Moreover, as the damaged degrees of the broken Propellers of category 3 and 4 are heavier than the counterparts of category 2 and 5, the feature differences between the training and testing samples of category 3 and 4 are greater than the counterparts of category 2 and 5.

In addition, all-category difference features learned by DDCNN+DA on testing Dataset C are plotted together in Fig. 8. As shown, the features of five categories are different from each other, which makes it easier for the classifier to make the correct classification. Moreover, the magnitudes of the difference features are different for each category. We observe that when the magnitudes of the difference features are large,

the corresponding damage level of the propeller is also severe. Specifically, according to Fig. 5a, the damage level  $DL$  for the five labels are  $DL_3 \approx DL_4 > DL_2 > DL_5 > DL_1$ , while in Fig. 8, the peak value  $PV$  of the difference features for the five labels are  $PV_3 \approx PV_4 > PV_2 > PV_5 > PV_1$  as well. This observation provides a direction for calculating the damage level of broken propellers.

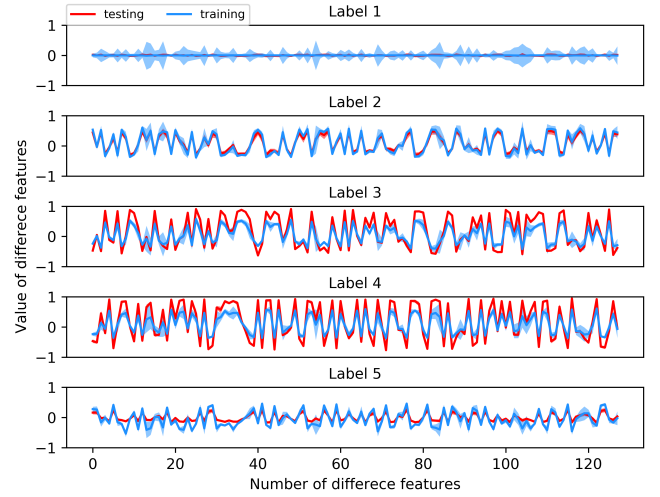


Fig. 7. Visualization of difference features of each category learned by DDCNN+DA on training Dataset A and testing Dataset C.

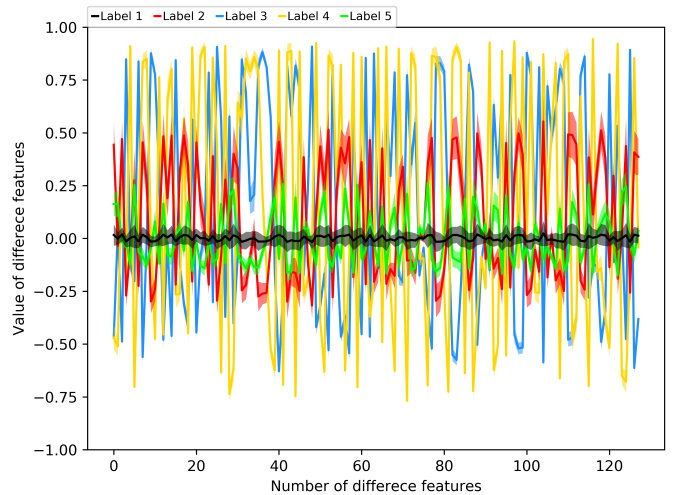


Fig. 8. Visualization of all-category difference features learned by DDCNN+DA on testing Dataset C.

## VI. CONCLUSION

In this paper, the proposed approach successfully solved the sim-to-real UAV fault diagnosis problem. With the proposed DDCNN model and the domain adaptation method, the trained classifier can achieve an average accuracy of about 98%. Through feature visualization, it is better understand why our DDCNN+DA model performs well in sim-to-real fault diagnosis tasks. Inspired by the observations in Section V-D, in the future, we plan to use the difference features learned by DDCNN to predict the damage level of the broken propeller.

## REFERENCES

- [1] H. Shraim, A. Awada, and R. Youness, "A survey on quadrotors: Configurations, modeling and identification, control, collision avoidance, fault diagnosis and tolerant control," *IEEE Aerospace and Electronic Systems Magazine*, vol. 33, no. 7, pp. 14–33, 2018.
- [2] J. A. Guzmán-Rabasa, F. R. López-Estrada, B. M. González-Contreras, G. Valencia-Palomo, M. Chadli, and M. Perez-Patricio, "Actuator fault detection and isolation on a quadrotor unmanned aerial vehicle modeled as a linear parameter-varying system," *Measurement and Control*, vol. 52, no. 9-10, pp. 1228–1239, 2019.
- [3] M. H. Amoozgar, A. Chamseddine, and Y. Zhang, "Experimental test of a two-stage Kalman filter for actuator fault detection and diagnosis of an unmanned quadrotor helicopter," *Journal of Intelligent & Robotic Systems*, vol. 70, no. 1, pp. 107–117, 2013.
- [4] G. Iannace, G. Ciaburro, and A. Trematerra, "Fault diagnosis for UAV blades using artificial neural network," *Robotics*, vol. 8, no. 3, p. 59, 2019.
- [5] J. Park, Y. Jung, and J.-H. Kim, "Multiclass Classification Fault Diagnosis of Multirotor UAVs Utilizing a Deep Neural Network," *International Journal of Control, Automation and Systems*, vol. 20, no. 4, pp. 1316–1326, 2022.
- [6] G. E. Hinton and R. R. Salakhutdinov, "Reducing the dimensionality of data with neural networks," *science*, vol. 313, no. 5786, pp. 504–507, 2006.
- [7] W. Zhang, C. Li, G. Peng, Y. Chen, and Z. Zhang, "A deep convolutional neural network with new training methods for bearing fault diagnosis under noisy environment and different working load," *Mechanical Systems and Signal Processing*, vol. 100, pp. 439–453, 2018. [Online]. Available: <http://dx.doi.org/10.1016/j.ymssp.2017.06.022>
- [8] W. Zhang, Y. Zhang, N. Liu, K. Ren, and P. Wang, "IPAPRec: A promising tool for learning high-performance mapless navigation skills with deep reinforcement learning," *IEEE/ASME Transactions on Mechatronics*, vol. 27, no. 6, pp. 5451–5461, 2022.
- [9] P. Yang, H. Geng, C. Wen, and P. Liu, "An Intelligent Quadrotor Fault Diagnosis Method Based on Novel Deep Residual Shrinkage Network," *Drones*, vol. 5, no. 4, p. 133, 2021.
- [10] S. S. Katta, K. Vuojärvi, S. Nandyala, U.-M. Kovalainen, and L. Baddeley, "Real-World On-Board Uav Audio Data Set For Propeller Anomalies," in *ICASSP 2022-2022 IEEE International Conference on Acoustics, Speech and Signal Processing (ICASSP)*. IEEE, 2022, pp. 146–150.
- [11] Y. LeCun, Y. Bengio, and others, "Convolutional networks for images, speech, and time series," *The handbook of brain theory and neural networks*, vol. 3361, no. 10, p. 1995, 1995.
- [12] A. Vaswani, N. Shazeer, N. Parmar, J. Uszkoreit, L. Jones, A. N. Gomez, L. Kaiser, and I. Polosukhin, "Attention is all you need," *Advances in neural information processing systems*, vol. 30, 2017.
- [13] L. Tai, G. Paolo, and M. Liu, "Virtual-to-real deep reinforcement learning: Continuous control of mobile robots for mapless navigation," in *IEEE International Conference on Intelligent Robots and Systems*, vol. 2017-Sept, 2017, pp. 31–36.
- [14] W. Zhang, N. Liu, and Y. Zhang, "Learn to Navigate Maplessly with Varied LiDAR Configurations: A Support Point-Based Approach," *IEEE Robotics and Automation Letters*, 2021.
- [15] B. Rubí, B. Morcego, and R. Pérez, "Quadrotor Path Following and Reactive Obstacle Avoidance with Deep Reinforcement Learning," *Journal of Intelligent and Robotic Systems: Theory and Applications*, vol. 103, no. 4, 2021.
- [16] P. Zieliński and U. Markowska-Kaczmar, "3D robotic navigation using a vision-based deep reinforcement learning model," *Applied Soft Computing*, vol. 110, p. 107602, 2021.
- [17] A. Loquercio, E. Kaufmann, R. Ranftl, A. Dosovitskiy, V. Koltun, and D. Scaramuzza, "Deep Drone Racing: From Simulation to Reality with Domain Randomization," *IEEE Transactions on Robotics*, vol. 36, no. 1, pp. 1–14, 2020.
- [18] D. Chicco, "Siamese neural networks: An overview," *Artificial Neural Networks*, pp. 73–94, 2021.
- [19] L. Wen, X. Li, L. Gao, and Y. Zhang, "A New Convolutional Neural Network-Based Data-Driven Fault Diagnosis Method," *IEEE Transactions on Industrial Electronics*, vol. 65, no. 7, pp. 5990–5998, 2018.
- [20] J. J. Tong, W. Zhang, F. Liao, C. F. Li, and Y. F. Zhang, "Machine Learning for UAV Propeller Fault Detection based on a Hybrid Data Generation Model," *arXiv preprint arXiv:2302.01556*, 2023.